Silicene for Na-ion battery applications

To cite this article: Jiajie Zhu and Udo Schwingenschlögl 2016 *2D Mater.* **3** 035012

2D Materials

PAPER

Silicene for Na-ion battery applications

RECEIVED
26 June 2016

REVISED
28 July 2016

ACCEPTED FOR PUBLICATION
10 August 2016

PUBLISHED
19 August 2016

Jiajie Zhu and Udo Schwingenschlögl

King Abdullah University of Science and Technology (KAUST), Physical Science and Engineering Division (PSE), Thuwal 23955-6900, Saudi Arabia

E-mail: udo.schwingenschlogl@kaust.edu.sa

Keywords: silicene, graphene, Na-ion battery

Abstract

Na-ion batteries are promising candidates to replace Li-ion batteries in large scale applications because of the advantages in natural abundance and cost of Na. Silicene has potential as the anode in Li-ion batteries but so far has not received attention with respect to Na-ion batteries. In this context, freestanding silicene, a graphene-silicene-graphene heterostructure, and a graphene-silicene superlattice are investigated for possible application in Na-ion batteries, using first-principles calculations. The calculated Na capacities of 954 mAh/g for freestanding silicene and 730 mAh/g for the graphene-silicene superlattice (10% biaxial tensile strain) are highly competitive and potentials of >0.3 V against the Na^+/Na potential exceed the corresponding value of graphite. In addition, the diffusion barriers are predicted to be <0.3 eV.

1. Introduction

Renewable, environmentally friendly, and cheap energy sources become more and more important due to the rapidly growing energy consumption. Li-ion batteries are key components for energy storage, providing excellent performance, in particular a high energy density, absence of memory effects, and a long cycle life [1–6]. They are widely used in portable electronic devices such as cell phones and laptops. However, the scarcity and high cost of Li limit their field of applications. Na-ion batteries are considered to be promising alternatives because of the similarity of Na to Li. The natural abundance and low cost of Na makes Na-ion batteries especially suitable for large scale applications, in particular electric vehicles and power grids [7].

Graphite is the commercial anode material for Li-ion batteries, providing a long cycle life and being cost efficient, but is not suitable for Na-ion batteries due to a low capacity [8]. Although expanded graphite can improve the capacity to 284 mAh/g [9], the low electrode potential of 0.3 V against the Na^+/Na potential causes safety issues of dendritic Na growth, especially at high cycling rates [10]. Therefore, considerable effort has been put into the search for and design of new anode materials. P and Sn show high Na capacities of 2596 mAh/g [11] and 847 mAh/g [12], respectively, but the huge volume change of ~500% during the alloying-dealloying reaction leads to disintegration of the anode and formation of excessively thick solid electrolyte interphase layers, which eventually results in a capacity loss as well as in safety concerns [13].

Dimensional reduction from bulk to two or one-dimensional materials can significantly improve the charging-discharging performance, as has been demonstrated for P and Sn-based anodes [13, 14]. Two-dimensional materials typically perform better than one-dimensional materials, due to the higher structural stability [15], and therefore are attracting recent attention. For MXenes Na capacities of up to 288 mAh/g [16] have been predicted. However, surface functional groups, such as F, O, and OH, will obstruct the ion migration [17]. A high Na capacity of 865 mAh/g and a low diffusion barrier of 0.04 eV have been predicted for freestanding phosphorene [18], regrettably combined with a large band gap that leads to low conductivity [5]. While Si-Na alloys have been addressed [19], silicene so far has not received attention with respect to Na-ion batteries. On the other hand, a promising performance of silicene, including a high capacity of 954 mAh/g and a low diffusion barrier of 0.23 eV, has been predicted for Li-ion batteries [20]. Enhanced interaction of Na with silicene as compared to graphite leads to a higher electrode potential, which suppresses dendritic Na growth [10, 20, 21].

Graphene-silicene heterostructures are characterized by a small lattice mismatch and predicted to be stable at room temperature [22, 23]. In addition, the Dirac states turn out to be preserved. Both the high stiffness of graphene and the large interlayer separation in the heterostructure can be expected to be advantageous for accommodating the strain and volume expansion experienced during the charging-discharging process. Furthermore, the small atomic mass of graphene increases the Na capacity [24] and issues with the solid electrolyte interphase can be overcome by increasing the thickness of the heterostructure (smaller surface-to-volume ratio) [5]. We also notice that high Na capacities combined with stable cycling previously have been achieved in graphene/phosphorene hybrid materials [25]. For these reasons, we will investigate in the present work the suitability of silicene as anode material for Na-ion batteries.

2. Computational method

All the simulations discussed in the following are performed within density functional theory and the projector augmented wave method, as implemented in Vienna Ab-initio Simulation Package [26]. The generalized gradient approximation as proposed by Perdew, Burke and Ernzerhof is selected for handling the exchange-correlation potential [27]. In addition, the long-range interlayer interaction between graphene and silicene is taken into account by means of the DFT-D3 van der Waals correction [28]. We set the plane wave cut-off energy to 500 eV and the energy criterion for the self-consistency iteration to 10^{-6} eV. All structures are relaxed until the residual forces on the atoms have declined to <0.01 eV/Å. In order to investigate sodiation, $2 \times 2 \times 1$ supercells are built and complemented by vacuum layers of 15 Å thickness in the out-of-plane direction to avoid artificial interaction between periodic images. A $6 \times 6 \times 1$ k-mesh is used for the Brillouin zone integration, which has been carefully tested for convergence, as have all other technical parameters. Diffusion paths and barriers are determined by means of the nudged elastic band method [29] with 9 images between the initial and final locations.

3. Results and discussion

Atomic structures of sodiated freestanding (F) silicene and a graphene-silicene-graphene (GSG) heterostructure are shown in figure 1 for different lateral configurations, with the Na atoms on top of Si atoms in the lower/upper sublattice or on top of a hollow site (H). Configuration F-H turns out to be the ground state with energy differences of 0.16 eV and 0.26 eV per Na atom to configuration F-L and F-U, respectively, which agrees with previous theoretical results [30]. In configuration F-H the silicene buckling height is calculated to be 0.59 Å, which is larger than without Na attached (0.44 Å), and a distance of 1.91 Å separates Na from silicene. In configurations F-L and F-U the silicene buckling height is much larger, 0.77 Å and 0.95 Å, respectively. Without Na attached the GSG heterostructure shows an interlayer distance of 3.49 Å (with previous theoretical results ranging from 3.3 Å to 3.6 Å for different exchange-correlation potentials [22, 31]) and an enhanced silicene buckling height of 0.61 Å due to the interaction between graphene and silicene. The silicene buckling height of 1.05 Å in configuration GSG-H is much larger than in configuration F-H, reflecting an enhanced interaction between Na and silicene. Configurations GSG-L and GSG-U turn out to be unstable, as Na moves towards the hollow site.

Since the lifetime of Na-ion batteries is sensitive to the volume change during the charging-discharging process, we investigate the lattice expansion (zero stress condition) as a function of the Na coverage, see figure 2. In the case of freestanding silicene the lattice constant initially decreases from 3.87 Å to 3.80 Å when the coverage grows to 1 Na atom per silicene unit cell, i.e., the buckling of silicene is enhanced, even though the Na-Na repulsion grows. For higher Na coverage the lattice constant starts increasing up to a value of 3.88 Å for full sodiation (2 Na atoms per silicene unit cell). The GSG heterostructure shows a lattice constant of 3.72 Å without Na attached, due to the lattice mismatch between graphene and silicene. The modification during sodiation turns out to be much smaller (0.5%) than in the case of freestanding silicene (2.1%), which reflects the high stiffness of graphene.

Freestanding silicene and the GSG heterostructure can accommodate a maximum of 2 and 2.25 Na atoms per silicene unit cell, respectively. Enhancement of the maximal coverage by interaction with graphene previously has been reported for MoS_2-based Li-ion batteries [32]. The obtained Na capacities are 954 mAh/g and 367 mAh/g, see table 1, the former value for freestanding silicene being the same as reported for Li-ion batteries [20]. Extension of the GSG heterostructure to a graphene-silicene (GS) superlattice (alternating graphene and silicene sheets) enhances the Na capacity to 547 mAh/g. Although the structural integrity does not become an issue when additional Na atoms are introduced, Na clusters will form because of the limited space at the interface. Such clusters cannot be decomposed during the desodiation processes.

We find no improvement of the Na capacity of freestanding silicene up to 10% biaxial tensile strain. The GSG heterostructure, on the other hand, can accommodate 2.75 and 3 Na atoms per silicene unit cell under 5% and 10% biaxial tensile strain, respectively. Ab-initio molecular dynamics simulations at 300 K for 2 ps with a time step of 1 fs show distinct structural distortions, see figure 3, but the integrity is maintained and the Na atoms do not

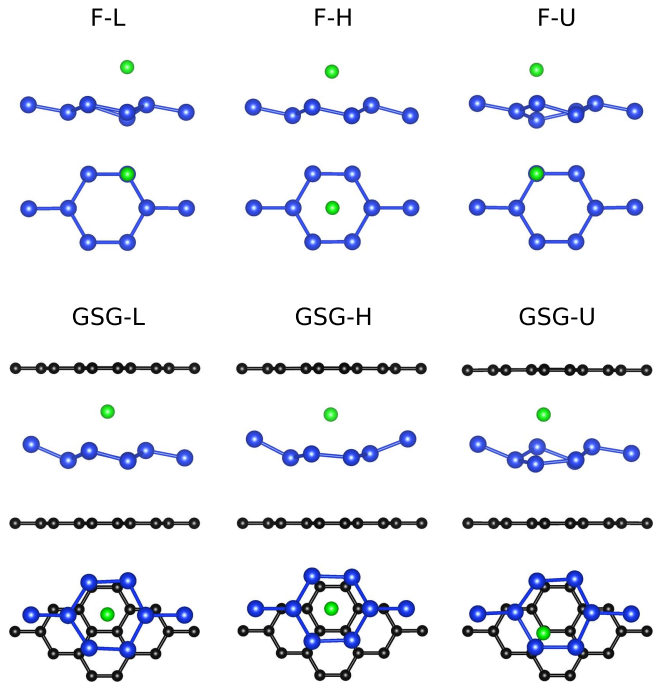

Figure 1. Side and top views of the sodiated silicene (top) and GSG heterostructure (bottom). The Si, C, and Na atoms are shown in blue, black, and green.

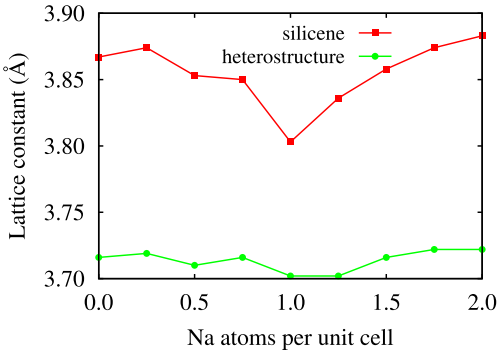

Figure 2. In-plane lattice constant as a function of the Na coverage.

Table 1. Na capacities (in mAh/g) for freestanding silicene, the GSG heterostructure, and a GS superlattice, under biaxial tensile strain.

	0% strain	5% strain	10% strain
silicene	954	954	954
heterostructure	367	449	490
superlattice	547	669	730

form clusters. The ultimate Na capacity that can be achieved in a GS superlattice amounts to 730 mAh/g, which is much larger than in the case of expanded graphite (284 mAh/g) and reported for Sn-based materials [9]. Importantly, we find that the volume expansion is only 20% (due to the increased interlayer distance), as compared to ∼500% in the case of bulk Sn [13].

The interaction in the different systems can be analyzed by means of the charge density difference $\Delta\rho = \rho_{\text{sodiated}} - \rho_{\text{non-sodiated}} - \rho_{\text{Na}}$ shown in figure 4, given by the charge densities of the sodiated system, the non-sodiated system, and a Na atom. In each case we find a pronounced redistribution of charge around Na. The amount of charge transfer between the components, calculated by the Bader approach, is summarized in table 2. Only in the case of the GSG heterostructure the charge transfer can be tuned by means of biaxial tensile strain. The distance between Na and silicene increases under strain, as the silicene buckling height decreases, see table 3, whereas the distance between Na and graphene remains almost constant. Accordingly, graphene (silicene) obtains more (less) charge, reflecting an increasing (decreasing) interaction.

This influences the open circuit voltage, given by $\text{OCV} = -\Delta H/n$, with ΔH and n being the reaction enthalpy of sodiation and the number of Na atoms. A positive OCV (negative ΔH) represents stability after sodiation. For freestanding silicene without strain the OCV ranges from 0.3 V to 0.5 V, see figure 5, which is higher than in graphite-based Li-ion batteries (0.2 V against the Li^+/Li potential [10, 21]) and Na-ion batteries (0.3 V against the Na^+/Na potential [21]). Biaxial tensile strain is found to enhance the OCV. The values obtained for the GSG heterostructure are generally higher than for freestanding silicene. For coverages up to 1 Na atom per silicene unit cell the Na atoms prefer to be located on top of hollow sites, whereas for coverages from 1.5 to 2 Na atoms per silicene unit cell they favor the top of Si atoms

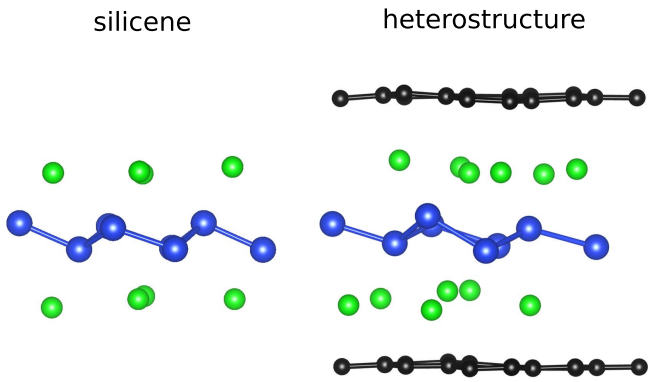

Figure 3. Snapshots (side view) of the fully sodiated freestanding silicene and GSG heterostructure under 10% biaxial tensile strain after 2 ps of ab-initio molecular dynamics simulations. The Si, C, and Na atoms are shown in blue, black, and green.

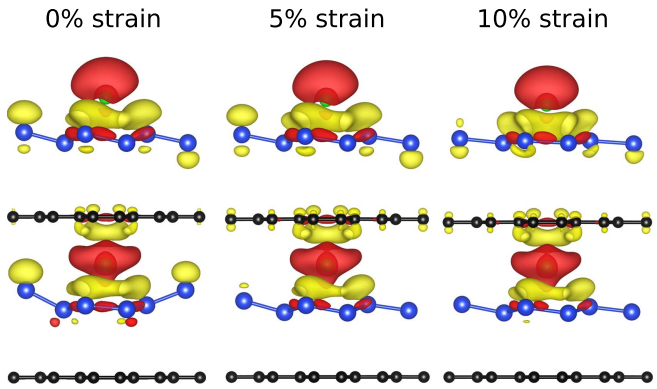

Figure 4. Charge density difference for the sodiated freestanding silicene (top) and GSG heterostructure (bottom) under biaxial tensile strain. Yellow/red represents charge accumulation/depletion with an isovalue of 10^{-3} electrons/bohr^3. The Si, C, and Na atoms are shown in blue, black, and green.

Table 2. Charge transfer (in electrons; calculated by the Bader approach) during the sodiation of freestanding silicene and the GSG heterostructure, for different amounts of biaxial tensile strain. Positive/negative values represent charge accumulation/depletion.

	silicene	graphene	Na
silicene			
0% strain	0.79	—	−0.79
5% strain	0.80	—	−0.80
10% strain	0.80	—	−0.80
heterostructure			
0% strain	0.55	0.25	−0.80
5% strain	0.36	0.46	−0.82
10% strain	0.27	0.55	−0.82

Table 3. Structural parameters (in Å) after sodiation of freestanding silicene and the GSG heterostructure, for different amounts of biaxial tensile strain: Si buckling height, distance between Na and silicene ($d_{\mathrm{Na-silicene}}$), and distance between Na and graphene ($d_{\mathrm{Na-graphene}}$).

	buckling height	$d_{\mathrm{Na-silicene}}$	$d_{\mathrm{Na-graphene}}$
silicene			
0% strain	0.59	1.91	—
5% strain	0.47	1.92	—
10% strain	0.30	1.92	—
heterostructure			
0% strain	1.05	1.36	2.59
5% strain	0.65	1.98	2.51
10% strain	0.49	2.09	2.50

in the lower sublattice. A reduction of the OCV is observed for high Na coverages, since the additional Na atoms again occupy hollow sites. The average Si buckling height increases with the Na coverage for freestanding silicene, which makes it more reactive. Domination of the Si-Na interaction over the Na-Na repulsion leads to an increased open circuit voltage for 0% and 5% biaxial tensile strain. On the other hand, as the distance between silicene and graphene increases with the Na coverage for the GSG heterostructure, the Na-Na repulsion reduces the open circuit voltage.

As the charging and discharging processes are determined by the Na diffusion barrier, we study three diffusion paths connecting neighboring Na ground state locations on silicene, see figure 6. Paths I and II pass on top of Si atoms in the lower and upper sublattice, respectively, while path III directly connects

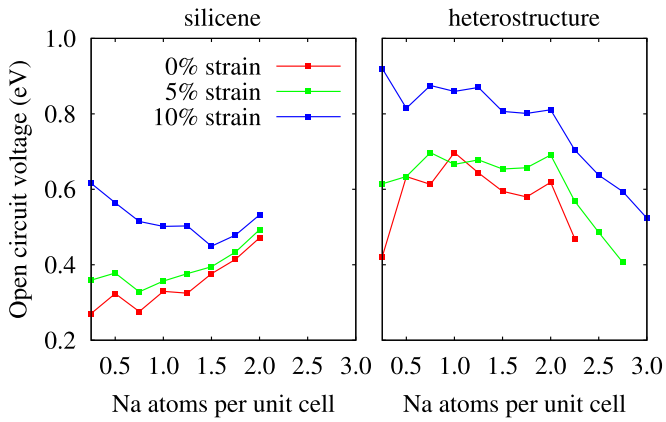

Figure 5. Open circuit voltage as function of the Na coverage, for different amounts of biaxial tensile strain.

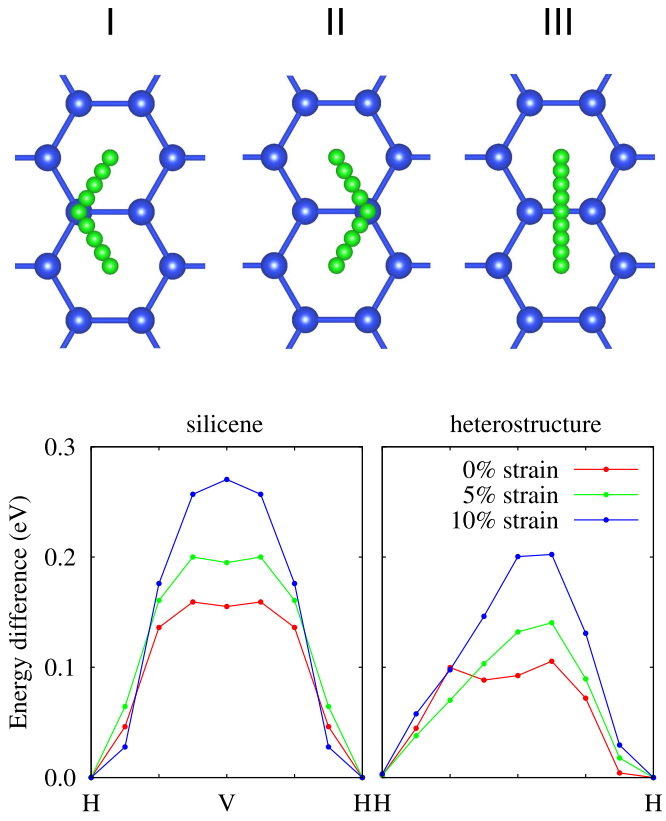

Figure 6. Na diffusion paths and barriers on freestanding silicene and in the GSG heterostructure, for different amounts of biaxial tensile strain.

the initial and final locations. Only path III is considered for the GSG heterostructure, since configurations GSG-L and GSG-U are unstable. Path I is found to result in the lowest diffusion barrier of 0.16 eV with the transition state located almost exactly on top of a Si atom in the lower sublattice. This value is lower than reported for Li diffusion on silicene (0.24 eV) [20] and graphite (0.22 eV) [21]. The diffusion barrier increases to 0.20 eV and 0.27 eV, respectively, under 5% and 10% biaxial tensile strain. For the GSG heterostructure a diffusion barrier of 0.11 eV is found, with the transition state near the middle of path III. This value is significantly lower than for Na diffusion in MoS_2 (0.28 eV) [33] and on B-doped graphene (0.16 eV to 0.22 eV) [34]. Enhanced diffusion barriers of 0.14 eV and 0.20 eV, respectively, are found under 5% and 10% biaxial tensile strain.

4. Conclusions

Silicene has been investigated by first-principles calculations to evaluate the applicability in Na-ion batteries. It turns out that sodiation leads to changes of the in-plane lattice constant by up to 2.1% for freestanding

silicene and 0.5% for the GSG heterostructure. The volume of a GS superlattice expands by only 20%. Importantly, the Na capacity is predicted to be 954 mAh/g for freestanding silicene and 730 mAh/g for the GS superlattice (10% biaxial tensile strain), which is much higher than in graphite and Sn-based materials. In addition, the Na diffusion barriers (0.16 eV for freestanding silicene and 0.11 eV for the GSG heterostructure) are significantly lower than in MoS_2 and B-doped graphene, for example. An OCV of >0.3 V is advantageous to avoid dendritic Na growth. Finally, biaxial tensile strain leads to charge transfer from silicene to graphene in the GSG heterostructure, which enhances both the Na capacity and diffusion barrier.

Acknowledgments

The research reported in this publication was supported by funding from King Abdullah University of Science and Technology (KAUST).

References

[1] Tang Q, Zhou Z and Shen P 2012 Are mxenes promising anode materials for Li ion batteries? computational studies on electronic properties and Li storage capability of Ti_3C_2 and $Ti_3C_2X_2$ (X = F, OH) monolayer *J. Am. Chem. Soc.* **134** 16909–16
[2] Li Y, Wu D, Zhou Z, Cabrera C R and Chen Z 2012 Enhanced Li adsorption and diffusion on MoS_2 zigzag nanoribbons by edge effects: a computational study *J. Phys. Chem. Lett.* **3** 2221–7
[3] Jing Y, Zhou Z, Cabrera C R and Chen Z 2013 Metallic VS_2 monolayer: a promising 2D anode material for lithium ion batteries *J. Phys. Chem.* C **117** 25409–13
[4] Jing Y, Ortiz-Quiles E O, Cabrera C R, Chen Z and Zhou Z 2014 Layer-by-layer hybrids of MoS_2 and reduced graphene oxide for lithium ion batteries *Electrochim. Acta* **147** 392–400
[5] Jing Y, Zhou Z, Cabrera C R and Chen Z 2014 Graphene, inorganic graphene analogs and their composites for lithium ion batteries *J. Mater. Chem.* A **2** 12104–22
[6] Sun W and Wang Y 2014 Graphene-based nanocomposite anodes for lithium-ion batteries *Nanoscale* **6** 11528–52
[7] Kang H, Liu Y, Cao K, Zhao Y, Jiao L, Wang Y and Yuan H 2015 Update on anode materials for Na-ion batteries *J. Mater. Chem.* A **3** 17899–913
[8] Doeff M M, Ma Y, Visco S J and De Jonghe L C 1993 Electrochemical insertion of sodium into carbon *J. Electrochem. Soc.* **140** L169–70
[9] Wen Y, He K, Zhu Y, Han F, Xu Y, Matsuda I, Ishii Y, Cumings J and Wang C 2014 Expanded graphite as superior anode for sodium-ion batteries *Nat. Commun.* **5** 4033
[10] Liu J, Lu P-J, Liang S, Liu J, Wang W, Lei M, Tang S and Yang Q 2015 Ultrathin Li_3VO_4 nanoribbon/graphene sandwich-like nanostructures with ultrahigh lithium ion storage properties *Nano Energy* **12** 709–24
[11] Kim Y, Park Y, Choi A, Choi N-S, Kim J, Lee J, Ryu J H, Oh S M and Lee K T 2013 An amorphous red phosphorus/carbon composite as a promising anode material for sodium ion batteries *Adv. Mater.* **25** 3045–9
[12] Komaba S, Matsuura Y, Ishikawa T, Yabuuchi N, Murata W and Kuze S 2012 Redox reaction of Sn-polyacrylate electrodes in aprotic Na cell *Electrochem. Commun.* **21** 65–8
[13] Qian J, Wu X, Cao Y, Ai X and Yang H 2013 High capacity and rate capability of amorphous phosphorus for sodium ion batteries *Angew. Chem. Inter. Ed.* **52** 4633–6
[14] Nam D-H, Kim T-H, Hong K-S and Kwon H-S 2014 Template-Free electrochemical synthesis of Sn nanofibers as high-performance anode materials for Na-ion batteries *ACS Nano* **8** 11824–35
[15] Xie J, Yang X, Zhou S and Wang D 2011 Comparing one- and two-dimensional heteronanostructures as silicon-based lithium ion battery anode materials *ACS Nano* **5** 9225–31
[16] Xie Y, DallAgnese Y, Naguib M, Gogotsi Y, Barsoum M W, Zhuang H L and Kent P R C 2014 Prediction and characterization of MXene nanosheet anodes for non-lithium-ion batteries *ACS Nano* **8** 9606–15
[17] Zhu J, Chroneos A and Schwingenschlögl U 2015 Nb-based MXenes for Li-ion battery applications *Phys. Status Solidi RRL* **9** 726–9
[18] Kulish V V, Malyi O I, Persson C and Wu P 2015 Phosphorene as an anode material for na-ion batteries: a first-principles study *Phys. Chem. Chem. Phys.* **17** 13921–8
[19] Morito H, Yamada T, Ikeda T and Yamane H 2009 Na-Si binary phase diagram and solution growth of silicon crystals *J. Alloys Compd.* **480** 723–6
[20] Tritsaris G A, Kaxiras E, Meng S and Wang E 2013 Adsorption and diffusion of lithium on layered silicon for Li-ion storage *Nano Lett.* **13** 2258–63
[21] Persson K, Hinuma Y, Meng Y S, Van der Ven A and Ceder G 2010 Thermodynamic and kinetic properties of the Li-graphite system from first-principles calculations *Phys. Rev.* B **82** 125416
[22] Neek-Amal M, Sadeghi A, Berdiyorov G R and Peeters F M 2013 Realization of free-standing silicene using bilayer graphene *Appl. Phys. Lett.* **103** 261904
[23] Berdiyorov G R, Neek-Amal M, Peeters F M and van Duin A C T 2014 Stabilized silicene within bilayer graphene: a proposal based on molecular dynamics and density-functional tight-binding calculations *Phys. Rev.* B **89** 024107
[24] Liu H, Gao J and Zhao J 2013 Silicene on substrates: a way to preserve or tune its electronic properties *J. Phys. Chem.* C **117** 10353–9
[25] Sun J, Lee H-W, Pasta M, Yuan H, Zheng G, Sun Y, Li Y and Cui Y 2015 A phosphorene-graphene hybrid material as a high-capacity anode for sodium-ion batteries *Nat. Nanotechnol* **10** 980–5
[26] Kresse G and Joubert D 1999 From ultrasoft pseudopotentials to the projector augmented-wave method *Phys. Rev.* B **59** 1758–75
[27] Perdew J P, Burke K and Ernzerhof M 1996 Generalized gradient approximation made simple *Phys. Rev. Lett.* **77** 3865–8
[28] Grimme S, Antony J, Ehrlich S and Krieg H A 2010 Consistent and accurate *ab initio* parametrization of density functional dispersion correction (DFT-D) for the 94 elements H-Pu *J. Chem. Phys.* **132** 154104
[29] Mills G, Jónsson H and Schenter G K 1995 Reversible work transition state theory: application to dissociative adsorption of hydrogen *Surf. Sci.* **324** 305–37
[30] Quhe R *et al* 2012 Tunable and sizable band gap in silicene by surface adsorption *Sci. Rep.* **2** 853
[31] Cai Y, Chuu C-P, Wei C M and Chou M Y 2013 Stability and electronic properties of two-dimensional silicene and germanene on graphene *Phys. Rev.* B **88** 245408
[32] Shu H, Li F, Hu C, Liang P, Cao D and Chen X 2016 The capacity fading mechanism and improvement of cycling stability in MoS_2-Based anode materials for lithium-ion batteries *Nanoscale* **8** 2918–26
[33] Mortazavi M, Wang C, Deng J, Shenoy V B and Medhekar N V 2014 Ab initio characterization of layered MoS_2 as anode for sodium-ion batteries *J. Power Sources* **268** 279–86
[34] Ling C and Mizuno F 2014 Boron-Doped graphene as a promising anode for Na-ion batteries *Phys. Chem. Chem. Phys.* **16** 10419–24